Optical and Photophysical Properties of Indolocarbazole Derivatives

Michel Belletête,[†] Nicolas Blouin,[‡] Pierre-Luc T. Boudreault,[‡] Mario Leclerc,[‡] and Gilles Durocher*[,†]

Laboratoire de Photophysique Moléculaire, Département de Chimie, Université de Montréal, C.P. 6128, Succ. Centre-Ville, Montréal, Québec, H3C 3J7, Canada, and Laboratoire des Polymères Photoactifs et Électroactifs, Centre de Recherche en Sciences et Ingénierie des Macromolécules (CERSIM), Université Laval, Cité Universitaire, Québec, G1K 7P4, Canada

Received: September 19, 2006; In Final Form: October 19, 2006

We present a study of the optical and photophysical properties of five ladder indolo[3,2-*b*]carbazoles, namely, **M1**, **M2**, **M3**, **M4**, and **M5**. The ground-state optimized structures were obtained by B3LYP/6-31G* density functional theory (DFT) calculations, whereas the optimization (relaxation) of the first singlet excited electronic state (S_1) was performed using the restricted configuration interaction (singles) (RCIS/6-31G*) approach. The excitation to the S_1 state does not cause important changes in the geometrical parameters of the compounds, as corroborated by the small Stokes shifts. The excitation and emission energies have been obtained by employing the time-dependent density functional theory (TDDFT). For all the compounds, excitation to the S_1 state is weakly allowed, whereas the $S_2 \leftarrow S_0$ electronic transition of each oligomer possesses a much larger oscillator strength. The absorption and fluorescence spectra of the compounds have been recorded in chloroform. A reasonable agreement is obtained between TDDFT vertical transition energies and the (0,0) absorption and fluorescence bands. On one hand, the pattern of the aliphatic side chains does not affect the absorption and fluorescence maxima of the compounds. On the other hand, the replacement of aliphatic chains by phenyl or thiophene rings induces hypsochromic shifts in the absorption and fluorescence spectra. Finally, the fluorescence quantum yield and lifetime of the compounds in chloroform have been obtained. From these data, the radiative and nonradiative rate constants of the deactivation of the S_1 state have been determined.

1. Introduction

Organic electronics is potentially one of the most important emerging new technologies.[1−8] The search for new materials with good performance characteristics as well as the improvement in device fabrication has been the subject of many investigations. Because of their good molecular packing,[9] thermal stability,[10] and charge carrier mobility,[11−13] ladder polymeric materials are good candidates for applications in micro-electronics and in photovoltaic cells (PCs).[14−16] On the basis of these physical properties, Leclerc's group recently has developed semiconducting organic materials based on ladder oligo(*p*-aniline) derivatives that show good *p*-type electrical transport.[17−19] Interestingly, studies have revealed mobilities up to 0.14 $cm^2\ V^{-1}\ s^{-1}$ with some indolo[3,2-*b*]carbazole derivatives,[20,21] which make these processable and stable materials among the most promising ones for applications in organic electronics.[22]

Quantum chemical calculations are an important tool to investigate the relation between the electronic structure and the optical properties of π-conjugated materials. Along these lines, in the past few years, we have reported a number of joint theoretical and experimental studies for fluorene[23−25] and carbazole derivatives.[26−28] More recently, we have applied the density functional theory (DFT) and the time-dependent functional theory (TDDFT) on several ladder oligo(*p*-aniline)s.[29,30] It was found that DFT calculations give good geometrical parameters, whereas TDDFT results provide a good evaluation of the bathochromic shifts observed in the absorption and fluorescence spectra caused by an increase in the conjugation length or by the presence of alkyl chains on the nitrogen atoms. The present work aims at studying the effect of functionalization on the nitrogen atoms of ladder indolocarbazoles on their optical and photophysical properties. Indeed, recent works have shown that the electrical transport of these derivatives is greatly affected by their substitutional pattern.[17−22] The ground states of all the oligomers were treated using the density functional theory with the B3LYP functional (DFT/B3LYP/6-31G*), and the excitation energies were calculated using the time-dependent density functional theory (TDDFT). Then the S_1 excited states are optimized using the restricted configuration interaction (singles) (RCIS/6-31G*) approach, and the $S_1 \rightarrow S_0$ electronic transitions from the relaxed excited states were obtained from TDDFT calculations using optimized excited states as inputs. Finally, the optical properties and photophysics of these derivatives have been measured in chloroform. The absorption and fluorescence spectra of the ladder indolocarbazoles (the ethyl chains are replaced by hexyl groups in the actual compounds) are correlated to the theoretical results. Reasonable agreement is obtained between the computed electronic transitions and the optical data. The photophysical results are discussed in terms of the relative importance of the radiative and nonradiative processes occurring in these materials. The five compounds investigated, namely, **M1**, **M2**, **M3**, **M4**, and **M5**, are depicted in Figure 1.

2. Experimental Procedures

2.1. Computational Details. All calculations of the ladder indolocarbazoles studied in this work have been performed using

* Author to whom correspondence should be addressed. Tel.: (514) 343-6911; fax: (514) 343-7586; e-mail: gilles.durocher@umontreal.ca.
[†] Université de Montréal.
[‡] Université Laval.

10.1021/jp066143a CCC: $33.50
Published on Web 12/02/2006

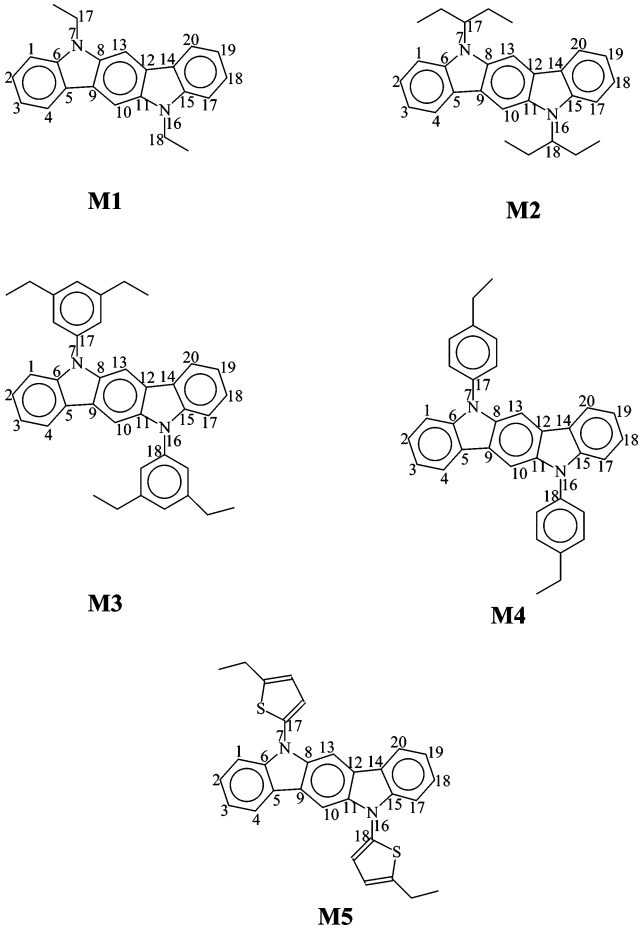

Figure 1. Molecular structure and numbering of the compounds investigated.

the *Gaussian 03* program package.[31] The ground-state geometry of each compound was determined by a full optimization of its structural parameters using the density functional theory (DFT).[32,33] There is no symmetric constraint on the geometric optimization. In the DFT method, electron correlation effects were taken into account, and this method is often used as a compromise for higher end calculations at a reasonable computational cost. In this work, the DFT calculations were performed using Becke's three-parameter hybrid functional, B3,[34] with nonlocal correlation of Lee−Yang−Parr, LYP, abbreviated as B3LYP[35] in conjunction with the 6-31G* split-valence polarized basis set.[36] It is well-understood that, in general, DFT/B3LYP/6-31G* calculations provide accurate geometries for conjugated derivatives.[37]

The nature and energy of the first two singlet−singlet electronic transitions have been obtained by TDDFT/B3LYP/6-31G* calculations[38,39] performed on the DFT/B3LYP/6-31G* optimized geometries. TDDFT using the B3LYP input proved to be accurate for evaluating the transition energies of many molecular systems.[40−43] The excited-state geometries (S_1) were optimized by ab initio RCIS/6-31G*.[44] On the basis of the S_1 optimized geometries, the $S_1 \rightarrow S_0$ electronic emission energies were computed at the TDDFT/B3LYP/6-31G* level.

2.2 Synthesis and Characterization. General. ^{1}H and ^{13}C NMR spectra were recorded on a Varian AS400 apparatus in an appropriated deuterated solvent solution at 298 K. Chemical shifts were reported as δ values (ppm) relative to internal tetramethylsilane.

Materials. All starting organic compounds were purchased from Aldrich, Alfa Aesar, or TCI America and used without further purification. All reactions were carried out under argon at 1 atm unless mentioned otherwise. Some reaction solvents were distilled before use (THF from sodium/benzophenone; diethyl ether from potassium/benzophenone; $CHCl_3$ from CaH_2; and MeOH from CaH_2). Column chromatography was carried out on a silica gel (size 40−63 μm, pore size 60 Å, Silicycle). The 5,11-dihydroindolo[3,2-*b*]carbazole (**1**),[45] 3,5-dibromo-1-trimethylsilylbenzene[46] purified by high vacuum distillation,[47] and 1-hexyl-4-iodobenzene[48] have been already reported in the literature. All other compounds have been synthesized following procedures described here.

Tridecan-7-ol (2). In a 1 L flame-dried round-bottomed flask fitted with a condenser and containing a magnetic stir bar, 20.00 g (100.8 mmol) of tridecan-7-one was dissolved in 250 mL of THF and cooled down to 0 °C. A total of 11.48 g (302.4 mmol) of $LiAlH_4$ was added slowly in small portions, and the resulting mixture was stirred at room temperature for 30 min and then refluxed overnight. The reaction mixture was allowed to cool to room temperature, and methanol was added slowly in small portions to destroy any remaining $LiAlH_4$ (caution: violent reaction), and then saturated NH_4Cl (100−150 mL) was added. The mixture was poured in distillated water (300 mL) and extracted 3 times with diethyl ether (250−300 mL). The combined organic layers were dried over $MgSO_4$, and the solvent was removed under reduced pressure to afford 19.12 g as the title product (Yield: 93%). The product was used without further purification as a colorless powder. mp 36−37 °C. ^{1}H NMR (400 MHz, $CDCl_3$, ppm): δ 3.58 (m, 1H); 1.66 (s, 1H); 1.42 (m, 6H); 1.27 (m, 14H); 0.87 (t, J = 7.1 Hz, 6H). ^{13}C NMR (100 MHz, $CDCl_3$, ppm): δ 72.13; 37.60; 32.04; 31.98; 29.52; 25.75; 22.75; 14.20. HRMS: Calcd for $C_{13}H_{26}$ (M − H_2O): 182.2034; found: 182.2040 ± 0.0005. Calcd for $C_{13}H_{27}O$ (M − H): 199.2062; found: 199.2065 ± 0.0006.

7-Tridecane *p*-Toluenesulfonate (3). In a flame-dried round-bottomed flask containing a magnetic stir bar, 5.000 g (25.00 mmol) of tridecan-7-ol (**2**) was dissolved in anhydrous pyridine (12.5 mL) and cooled at 0 °C with an ice bath. A total of 5.243 g (27.50 mmol) of *p*-toluenesulfonyl chloride was added slowly, and the mixture was stirred for 2 h at 0 °C before the ice bath was removed. After 4 h at room temperature, the reaction was poured into water (150 mL) and extracted twice with diethyl ether (150 mL). The combined organic layers were washed 5 times with 0.1 M $CuSO_4$ aqueous solution (100 mL), 2 times with brine (200 mL), and 1 time with water (250 mL). The organic layer was dried with $MgSO_4$, the solvent was removed under reduced pressure, and the crude product was purified by column chromatography (silica gel, 90% hexanes/10% ethyl acetate as eluent) to obtain 6.618 g as a colorless oil (yield: 75%). ^{1}H NMR (400 MHz, $CDCl_3$, ppm): δ 7.77 (d, J = 7.6 Hz, 2H); 7.31 (d, J = 7.7 Hz, 2H); 4.52 (qt, J = 5.7 Hz, 1H); 2.42 (s, 3H); 1.54 (m, 4H); 1.17 (m, 16H); 0.84 (t, J = 7.0 Hz, 6H). ^{13}C NMR (100 MHz, $CDCl_3$, ppm): δ 144.39; 134.85; 129.70; 127.79; 84.73; 34.21; 31.67; 29.03; 24.72; 22.57; 21.66; 14.13. HRMS: Calcd for $C_{20}H_{38}NO_3S$ (M + NH_4^+): 372.2572; found: 372.2577 ± 0.0011.

General Indolocarbazole Alkylation Procedure.[49] A flame-dried three necked flask fitted with a addition funnel and a magnetic stir bar was charged with 400 mg (1.561 mmol) of indolocarbazole, 3.75 mL of DMSO, and 876 mg (15.61 mmol) of powdered potassium hydroxide. When indolocarbazole was completely dissolved (reddish solution), a solution of 4.682 mmol of alkyl chains in DMSO (2.5 mL) was added dropwise through the addition funnel over 1−1.5 h at room temperature. After 6 h, the reaction was poured into 200 mL of distillated

water, and the aqueous layer was extracted 3 times with dichloromethane. The combined organic fractions were dried over magnesium sulfate, and the solvent was removed under reduced pressure. The crude product was dissolved in dichloromethane, preadsorbed on silica gel, and purified by column chromatography.

5,11-Di(hexyl)indolo[3,2-*b*]carbazole (M1). Following the general indolocarbazole alkylation procedure, 0.773 g (0.66 mL) of bromohexane afforded 0.601 g as the title product after column chromatography (85% hexanes/15% dichloromethane) (yield: 91%). Crystals were obtained by slow evaporation of an acetone solution. mp 143−145 °C. ^{1}H NMR (400 MHz, C_6H_6, ppm): δ 8.27 (d, J = 7.6 Hz, 2H); 8.09 (s, 2H); 7.50 (t, J = 7.4 Hz, 2H); 7.31 (t, J = 7.4 Hz, 2H); 7.27 (d, J = 8.3 Hz, 2H); 4.00 (t, J = 7.1 Hz, 4H); 1.66 (m, 4H); 1.16 (m, 4H); 1.08 (m, 8H); 0.79 (t, J = 6.6 Hz, 6H). ^{13}C NMR (100 MHz, C_6H_6, ppm): δ 142.33; 136.69; 126.07; 123.65; 123.57; 120.71; 118.48; 108.87; 99.30; 43.25; 31.85; 28.98; 27.27; 22.87; 14.23. HRMS: Calcd for $C_{30}H_{36}N_2$: 424.287849; found: 424.2885 ± 0.0013.

5,11-Di(7′-tridecanyl)indolo[3,2-*b*]carbazole (M2). Following the general indolocarbazole alkylation procedure, 1.660 g of **3** afforded 0.795 g as the title product after column chromatography (90% hexanes/10% dichloromethane) (yield: 82%). Crystals suitable for X-rays structure analysis were obtained by slow evaporation of a pentane and hexane (1:1) solution. mp 120−122 °C. ^{1}H NMR (400 MHz, C_6H_6, ppm): δ 8.50 (s, 0.25H); 8.46 (2, 0.25H); 8.33 (m, 0.5 H); 8.22 (m, 1H); 7.58 (m, 0.5H); 4.47 (m, 1.0H); 7.38 (m, 0.5H); 7.26 (m, 1.0H); 7.16 (m, 2H); 4.62 (m, 0.5H); 4.51 (m, 0.5H); 2.52 (m, 1H); 2.30 (m, 1H); 1.77 (m, 2H); 1.16 (m, 4H); 1.07 (m, 8H); 0.95 (m, 4H); 0.75 (t, J = 7.2 Hz, 6H). (Fractional protons are due to a phenomenon of atropisomerism[50−52].) ^{13}C NMR (100 MHz, C_6H_6, ppm): δ 143.97; 140.37; 138.38; 138.35; 134.34; 126.15; 125.73; 124.65; 124.48; 123.30; 123.03; 120.79; 120.46; 118.37; 111.50; 108.88; 102.08; 101.62; 99.38; 98.95; 56.69; 56.61; 34.15; 34.07; 31.92; 31.84; 29.64; 29.56; 27.21; 27.07; 22.96; 14.24. (Multiple carbon peaks are due to a phenomenon of atropisomerism[50−52]. Peaks could be missing, probably hidden by the solvent peaks.) HRMS: Calcd for $C_{44}H_{64}N_2$: 620.5069; found: 620.5078 ± 0.0019.

3,5-Dihexyl-1-trimethylsilylbenzene (4). A flame-dried three necked flask fitted with a condenser and containing a magnetic stir bar was charged with 23.70 g (76.93 mmol) of 3,5-dibromo-1-trimethylsilylbenzene, 25.00 g (192.3 mmol) of fresh hexyl boronic acid, 70.86 g (307.7 mmol) of $K_3PO_4 \cdot H_2O$, 0.3454 g (1.539 mmol) of $Pd(OAc)_2$, and 1.264 g (3.078 mmol) of 2-dicyclohexylphosphino-2′,6′-dimethoxybiphenyl (SPhos) and was then carefully evacuated and backfilled with argon (this sequence was repeated 3 times). Carefully degassed toluene (150 mL) with argon over 30 min was added via a syringe through the septum, and the resulting mixture was heated at 100 °C with vigorous stirring overnight. The black reaction mixture was allowed to cool to room temperature, filtered through a thin pad of silica gel (eluting with hexanes), and concentrated under reduced pressure. Hexanes (500 mL) were added to the resulting oil and removed under reduced pressure to eliminate the remaining toluene. This operation was repeated 2 times, and the product was dried under reduced pressure overnight to afford 20.78 g of the title product as a colorless oil (yield: 85%). ^{1}H NMR (400 MHz, $CDCl_3$, ppm): δ 7.15 (s, 2H); 7.00 (s, 1H); 2.59 (dd, J_1 = 7.7 Hz and J_2 = 7.9 Hz, 4H); 1.62 (m, 4H); 1.33 (m, 12H); 0.90 (t, J = 6.7 Hz, 6H); 0.27 (s, 9H). ^{13}C NMR (100 MHz, $CDCl_3$, ppm): δ 142.18; 140.15; 130.85; 129.28; 36.26; 31.90; 31.84; 29.36; 22.79; 14.27; −0.86. HRMS: Calcd for $C_{21}H_{38}Si$: 318.2743; found: 318.2748 ± 0.009.

3,5-Dihexyl-1-iodobenzene (5). In a flame-dried round-bottomed flask, 24.00 g (77.90 mmol) of compound **4** was dissolved in anhydrous methanol (78 mL) and anhydrous chloroform (78 mL), and 33.52 g (163.6 mmol) of silver trifluoroacetate was added. The reaction was cooled down to 0 °C, and 39.54 g of iodine (155.8 mmol) was added all at once. Within 30−60 min, the reaction was completed by TLC analysis and filtered through Celite (washing with 750−1000 mL of additional hexanes). The solvent was evaporated, and the crude product was dissolved in hexanes (300 mL) and then washed 3 times with saturated sodium thiosulfate (450 mL) and then 2 times with water (450 mL). The organic layer was dried with $MgSO_4$, and the solvent removed under reduced pressure. The oil was purified by short column chromatography (silica gel, hexanes as eluent) to obtained 26.39 g of colorless oil as a final product (yield: 91%). ^{1}H NMR (400 MHz, $CDCl_3$, ppm): δ 7.35 (s, 2H); 6.94 (s, 1H); 2.51 (t, J = 7.8 Hz, 4H); 1.57 (m, 4H); 1.30 (m, 12H); 0.89 (t, J = 6.3 Hz, 6H). ^{13}C NMR (100 MHz, $CDCl_3$, ppm): δ 145.27; 134.77; 128.20; 94.57; 35.67; 31.81; 31.45; 29.09; 22.73; 14.24. HRMS: Calcd for $C_{18}H_{29}I$: 372.1314; found: 372.1308 ± 0.0011.

5-Hexylthiophene (6). A 500 mL flame-dried round-bottomed flask was charged under argon atmosphere with 15.00 g (14.1 mL, 178.3 mmol) of thiophene and 150 mL of anhydrous THF. The mixture was cooled to −78 °C, and 58.0 mL (0.144 mol) of *n*-BuLi (2.5 M in hexanes) was added drowise over 15 min. The resulting mixture was stirred for 45 min at this temperature, and then 22.30 g (19.0 mL, 135.1 mmol) of 1-bromohexane was added dropwise. The solution was warmed to room temperature and stirred for 3 h. The solution was dropped in water and extracted with diethyl ether (3 × 150 mL). The organic fractions were combined and dried over magnesium sulfate, and the solvent was removed under reduced pressure. The residue was purified by in vacuo distillation to afford 12.87 g of the title product as a colorless oil (yield: 57%). ^{1}H NMR (400 MHz, $CDCl_3$, ppm): δ 7.08 (d, J = 5.1 Hz, 1H); 6.90 (t, J = 4.4 Hz, 1H); 6.76 (d, J = 2.7 Hz, 1H); 2.80 (t, J = 7.8 Hz, 2H); 1.65 (m, 2H); 1.32 (m, 6H); 0.87 (t, J = 6.6 Hz, 3H). ^{13}C NMR (100 MHz, $CDCl_3$, ppm): δ 145.90; 126.72; 124.01; 122.83; 31.99; 31.80; 30.11; 29.02; 22.81; 14.27. HRMS: Calcd for $C_{10}H_{16}S$: 168.0973; found: 168.0970 ± 0.0005.

2-Iodo-5-hexylthiophene (7). A flame-dried round-bottomed flask was charged under argon atmosphere with 10.50 g (62.39 mmol) of 2-hexylthiophene (**6**) and 60 mL of anhydrous THF. The mixture was cooled to −78 °C, and 25.2 mL (63.00 mmol) of *n*-BuLi (2.5M in hexanes) was added dropwise over 15 min. The solution was warmed to 0 °C and added dropwise to a solution of 19.24 g (68.26 mmol) of 1,2-diiodoethane in 60 mL of anhydrous THF. The solution was stirred at this temperature for 2 h and partitioned between 200 mL of hexanes/diethyl ether (1:1). The organic layer was washed successively with an aqueous solution of sodium bicarbonate, sodium thiosulfate, and brine and dried over sodium sulfate. The solvent was removed under reduced pressure, and the crude product was purified by distillation under reduced pressure to afford 14.35 g of the title product as an orange oil (yield: 78%). ^{1}H NMR (400 MHz, $CDCl_3$, ppm): δ 7.02 (d, J = 3.6 Hz, 1H); 6.45 (d, J = 3.6 Hz, 1H); 2.77 (t, J = 7.5 Hz, 2H); 1.61 (m, 2H); 1.31 (m, 6H); 0.86 (t, J = 6.9 Hz, 3H). ^{13}C NMR (100 MHz, $CDCl_3$, ppm): δ 152.19; 136.61; 125.91; 69.64; 31.70; 31.65; 30.39; 28.87; 22.75; 14.31. HRMS: Calcd for $C_{10}H_{15}SI$: 293.9939; found: 293.9935 ± 0.0009.

General Indolocarbazole Arylation Procedure.[53,54] A flame-dried three necked flask fitted with a condenser and a thermometer was charged with 400 mg (1.561 mmol) of indolocarbazole, 27 mg (0.142 mmol) of CuI, 33 mg (0.284) of L-proline, 1.633 g (14.188 mmol) of anhydrous K_2CO_3, and 2.834 mmol of iodoaryl and then was carefully evacuated and backfilled with argon (this sequence was repeated 3 times). Degassed anhydrous dimethylsulfoxide (5.7 mL) via three freeze−pump−thaw cycles was added through the septum, and the mixture was heated at 85 °C (90 °C maximum) with an oil bath until reaction completion by TLC analysis or 72 h. The reaction mixture was then allowed to cool to room temperature, poured in 250 mL of distillated water, and extracted 3 times with dichloromethane. The combined organic layers were dried over $MgSO_4$, and the solvent was removed under reduced pressure. The crude product was dissolved in dichloromethane, preadsorbed on silica gel, and purified by column chromatography.

5,11-Di(4′-hexylbenzene)indolo[3,2-*b*]carbazole (M3). Following the general indolocarbazole arylation procedure, 4-hexyliodobenzene afforded 0.610 g as the title product after column chromatography (85% hexanes/15% dichloromethane) (yield: 71%). Crystals were obtained by slow evaporation of a pentane and hexane (1:1) solution. mp 148−152 °C. ^{1}H NMR (400 MHz, C_6H_6, ppm): δ 8.30 (s, 2H); 7.87 (d, $J = 7.7$ Hz, 2H); 7.41 (d, $J = 8.1$ Hz, 2H); 7.36 (d, $J = 8.2$ Hz, 2H); 7.33 (t, $J = 7.6$ Hz, 2H); 7.19 (t, $J = 7.4$ Hz,2H); 7.16 (m, 6H); 2.56 (t, $J = 7.7$ Hz, 4H); 1.61 (m, 4H); 1.30 (m, 12H); 0.93 (t, $J = 6.5$ Hz, 6H). ^{13}C NMR (100 MHz, C_6H_6, ppm): δ 142.97; 142.25; 137.98; 136.49; 130.20; 127.69; 126.37; 124.13; 124.12; 120.91; 119.65; 109.97; 100.51; 36.07; 32.14; 31.92; 29.50; 23.04; 14.39. HRMS: Calcd for $C_{42}H_{44}N_2$: 576.3504; found: 576.3509 ± 0.0017.

5,11-Di(3′,5′-dihexylbenzene)indolo[3,2-*b*]carbazole (M4). Following the general indolocarbazole alkylation procedure, **5** afforded 0.814 g as the title product after column chromatography (90% hexanes/10% dichloromethane) (yield: 77%). Crystals suitable for X-ray structure analysis were obtained by slow evaporation of a pentane and ethanol solution. mp 78−80 °C. ^{1}H NMR (400 MHz, C_6H_6, ppm): δ 8.43 (s, 2H); 8.02 (d, $J = 7.7$ Hz, 2H); 7.54 (d, $J = 7.5$ Hz, 2H); 7.37 (t, $J = 7.7$ Hz, 2H); 7.23 (m, 6H); 7.10 (s, 2H); 2.56 (t, $J = 7.6$ Hz, 8H); 1.61 (m, 8H); 1.27 (m, 24H); 0.90 (t, $J = 6.9$ Hz). ^{13}C NMR (100 MHz, C_6H_6, ppm): δ 145.20; 143.11; 138.86; 138.11; 126.41; 125.26; 124.17; 120.90; 119.62; 110.16; 100.66; 36.24; 32.12; 31.95; 29.45; 23.06; 14.38. (One peak is missing, probably hidden by the solvent peaks.) HRMS: Calcd for $C_{54}H_{68}N_2$: 744.5382; found: 744.5399 ± 0.0022.

5,11-Di-2′-(5′-hexylthiophene)indolo[3,2-*b*]carbazole (M5). Following the general indolocarbazole arylation procedure, **7** afforded 0.275 g as the title product after column chromatography (100% hexanes) (yield: 33%). Crystals suitable for X-ray structure analysis were obtained by slow evaporation of a dichloromethane/hexane (1:1) solution. mp 106−108 °C. ^{1}H NMR (400 MHz, CD_2Cl_2, ppm): δ 8.11 (d, $J = 7.6$ Hz, 2H); 8.09 (m, 2H); 7.45 (m, 4H); 7.27 (m, 2H); 7.13 (d, $J = 3.5$ Hz, 2H); 6.93 (dd, $J_1 = 0.8$ Hz and $J_2 = 3.6$ Hz, 2H); 2.94 (t, $J = 7.8$ Hz, 4H); 1.81 (m, 4H); 1.43 (m, 12H); 0.94 (t, $J = 6.8$ Hz, 3H). ^{13}C NMR (100 MHz, CD_2Cl_2, ppm): δ 145.62; 143.81; 139.03; 136.65; 126.86; 125.47; 124.02; 120.66; 120.54; 11-.58; 100.97; 32,17; 32.16; 31.33; 29.44; 23.20; 14.45. HRMS: Calcd for $C_{38}H_{40}N_2S_2$: 588.2633; found: 558.2619 ± 0.0017.

2.3. Spectral and Photophysical Measurements. Chloroform was supplied by A&C American Chemicals Ltd. (spectrograde) and used without any further purification. The purity of the solvent was confirmed by the absence of fluorescence at the maximum sensitivity of the spectrofluorometer. All experiments were carried out at room temperature.

UV−vis absorption spectra were recorded on a Varian Cary 1 Bio UV−vis spectrophotometer using 1 cm quartz cells and solute concentrations of $(1-2) \times 10^{-5}$ M. The molar extinction coefficients (ϵ) at absorption maxima were obtained from the slope of the absorbance versus the concentration using seven solutions of different concentrations. The emission spectra were recorded on a Spex Fluorolog-2 spectrofluorometer equipped with a 450 W Xe lamp and a Hamamatsu R928 photomultiplier tube. The spectra were recorded by keeping a 90° geometry and a bandpass of 2 nm in the excitation and emission monochromators. Each solution was excited near the wavelength of the absorption maximum using a 1 cm path length quartz cell. Solution concentrations used were $(1-2) \times 10^{-5}$ M, giving absorbances always less than 0.1 to avoid any inner-filter effects. For all molecules, a study of the concentration (C) effect was performed on the fluorescence intensity (I_F), and all measurements were performed in the linear region of the I_F versus C curve. Fluorescence excitation spectra of the compounds were recorded by collecting the emission at three different wavelengths and resemble UV−vis absorption spectrum. Fluorescence quantum yields were determined using 9,10-diphenylanthracene in cyclohexane as a standard ($\phi_f = 0.90$).[55] Fluorescence lifetimes were determined using the single-photon timing technique on commercially available Edinburgh Instrument, model 299T spectrometer equipped with a hydrogen-filled nanosecond flashlamp and the analysis software supplied by the manufacturer. Details on the instrument have been published elsewhere.[56] Theoretical equations were fitted to experimental data by means of a nonlinear weighted least-squares routine based on the Marquardt algorithm. The kinetic interpretation of the goodness-of-fit was assessed using plots of weighted residuals, reduced χ^2 values, and Durbin−Watson (DW) parameters.

3. Results and Discussion

3.1. Synthesis. The synthesis of compound **M1** to compound **M5** was performed according to the reaction shown in Figure 2. The alkyl chain **3** was prepared from a dihexyl ketone reduced by $LiAlH_4$ followed by a classical tosylation reaction in pyridine. Starting with 5,11-dihydroindolo[3,2b]carbazole,[45] the oligomers **M1** and **M2** were synthesized according to the Marzoni and Garbrecht[49] procedure. The precursor **4** was obtained from 3,5-dibromo-1-trimethylsilylbenzene[46] and carefully purified by high vacuum distillation[47] and hexyl boronic acid through Suzuki aryl−alkyl coupling developed by Buchwald et al.[57] The precursor **4** was converted to compound **5** using silver salt and iodine.[58] The compound **7** was prepared from lithiation of thiophene with *n*-butyl lithium followed by the addition of bromohexane and then was lithiated once again with *n*-butyl lithium and quenched with 1,2-iodoethane according to a similar procedure by Reich and Whipple.[59] The oligomers **M3**−**M5** were obtained using Ullmann's arylation developed by Ma et al.[53,54] catalyzed by L-PROLINE AND CUI.

3.2. Ground-State Structural Properties. The ground-state geometry of each compound was determined by a full optimization of its structural parameters using the DFT/B3LYP theoretical method. It was found that the DFT-optimized geometries were in excellent agreement with the data obtained from X-ray analyses.[60] Indeed, the standard deviation for bond lengths was 0.01 Å, whereas the standard deviation for bond angles was

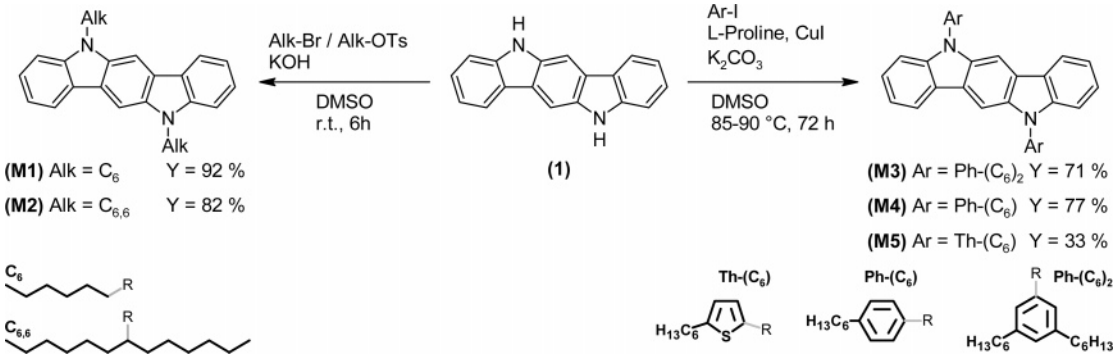

Figure 2. Synthesis for ladder oligo(*p*-aniline)s **M1**−**M5**.

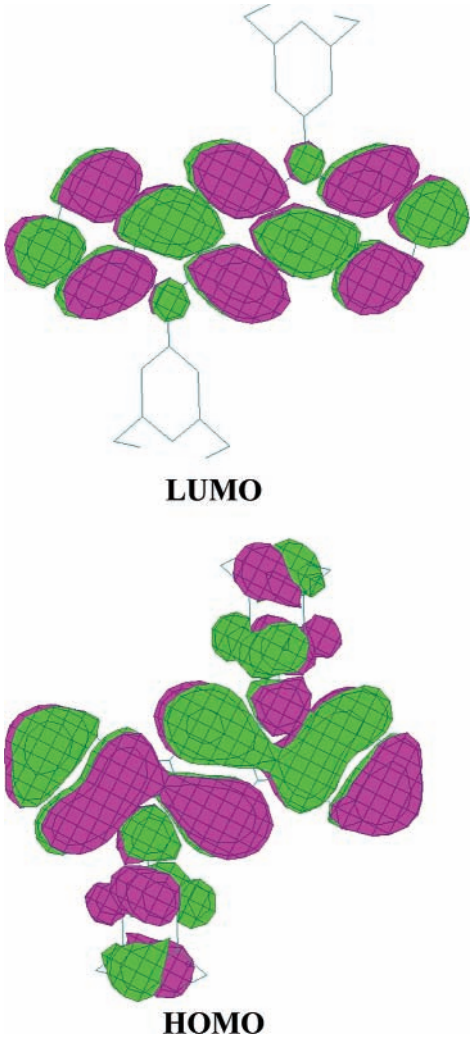

Figure 3. HOMO and LUMO isosurface plots of M3.

0.7°. It is also observed that the moieties on the nitrogen atoms are twisted (torsional angle >50°) with relatively high rotational barriers against planarity (E > 5 kcal mol^{-1}), when the molecules are in their ground electronic states (S_0).

3.3. Frontier Molecular Orbitals. It will be useful to examine the highest occupied and lowest virtual molecular orbitals of the indolocarbazoles because the relative ordering of the occupied and virtual orbitals provides a reasonable qualitative indication of the excitation properties[61] and of the ability of electron or hole transport. Because the first electronic transition corresponded mainly to the promotion of an electron from HOMO to LUMO, we have only drawn the isosurface plots of these molecular orbitals.

TABLE 1: HOMO and LUMO Energies and HOMO−LUMO Energy Gap of Ladder Indolo[3,2-*b*]carbazoles as Obtained from DFT/B3LYP/6-31G* Calculations

molecule	HOMO (eV)	LUMO (eV)	HOMO−LUMO (eV)
M1	−4.761	−0.974	3.787
M2	−4.682	−0.915	3.767
M3	−4.742	−0.932	3.810
M4	−4.768	−0.958	3.810
M5	−4.966	−1.005	3.960

It was observed that the functionalization of the compounds at the nitrogen atoms does not significantly affect the overall electronic structure of the main core. Indeed, it was found that the HOMO and LUMO topologies and sizes of the five derivatives investigated were almost identical. As an example, Figure 3 represents the isosurface plot of the HOMO and LUMO of **M3**. One can see that the HOMO involves atoms of the phenyl rings, whereas the LUMO shows no contributions from the atoms of the side chains. Both molecular orbitals are of π type and spread over the whole conjugated backbone, and one can immediately recognize their carbazole-like character.[62] Furthermore, the HOMO possesses an antibonding character between the subunits, whereas the LUMO shows bonding character between the rings.

The energy of the HOMO and LUMO and the HOMO−LUMO energy gap are compiled in Table 1. From this table, it can be seen that the replacement of primary alkyl chains by secondary alkyl chains (**M1** vs **M2**) on the nitrogen atoms slightly destabilizes both the HOMO and the LUMO orbitals. However, Table 1 shows that the LUMO is less destabilized than the HOMO for **M2**. The overall effect is a small decrease in the HOMO−LUMO energy gap of **M2** as compared to that of **M1**. Similarly, the replacement of aliphatic side chains by phenyl groups (**M3**) destabilizes both the HOMO and the LUMO orbitals, but this time, the LUMO orbital shows a larger increase in energy. Consequently, a small increase is found for the HOMO−LUMO energy gap of **M3** as compared to that of **M1**. On the other hand, the replacement of aliphatic side chains by thiophene groups (**M5**) stabilized both the HOMO and the LUMO orbitals but the LUMO to a much lesser extent. Thus, the overall effect is an increase of the HOMO−LUMO energy gap of **M5** as compared to that of **M1**. Finally, the change of the substitution pattern of the phenyl rings (that is, para vs meta) slightly stabilized HOMO and LUMO by the same amount, giving the same HOMO−LUMO energy gap for **M3** and **M4**.

3.4. Excitation Energies and Optical Properties. It is worth pointing out that HOMO−LUMO energy gaps are crude approximations to the transition energies. Indeed, the implicit assumption underlying this approximation is that the lowest singlet excited state can be described by only one singly excited

TABLE 2: Electronic Transition Data of ($S_1 \leftarrow S_0$) and ($S_2 \leftarrow S_0$) for Ladder Indolocarbazoles as Obtained by TDDFT/B3LYP/6-31G* Method Performed on DFT/B3LYP/6-31G* Optimized Geometries

molecule	transition	energy (cm^{-1})	f	MO/character	pol.	E_a[a] (cm^{-1})
M1	$S_1 \leftarrow S_0$	26 352	0.039	67% LUMO ← HOMO 13% LUMO + 2 ← HOMO-1	XY	23 900
	$S_2 \leftarrow S_0$	31 285	0.46	62% LUMO ← HOMO-1 26% LUMO + 2 ← HOMO	XY	29 200
M2	$S_1 \leftarrow S_0$	26 158	0.043	67% LUMO ← HOMO 13% LUMO + 2 ← HOMO-1	XY	23 900
	$S_2 \leftarrow S_0$	31 185	0.43	64% LUMO ← HOMO-1 26% LUMO + 2 ← HOMO	XY	29 200
M3	$S_1 \leftarrow S_0$	26 485	0.046	67% LUMO ← HOMO 13% LUMO + 6 ← HOMO-1	XY	24 400
	$S_2 \leftarrow S_0$	31 519	0.40	61% LUMO ← HOMO-1 17% LUMO + 2 ← HOMO	XY	29 400
M4	$S_1 \leftarrow S_0$	26 503	0.045	67% LUMO ← HOMO 13% LUMO + 2 ← HOMO-1	XY	24 500
	$S_2 \leftarrow S_0$	31 509	0.43	61% LUMO ← HOMO-1 24% LUMO + 6 ← HOMO 13% LUMO + 3 ← HOMO	XY	29 400
M5	$S_1 \leftarrow S_0$	27 699	0.056	67% LUMO ← HOMO 13% LUMO + 4 ← HOMO-1	XY	25 100
	$S_2 \leftarrow S_0$	31 779	0.58	63% LUMO ← HOMO-1 17% LUMO + 4 ← HOMO	XY	29 600

[a] Absorption energy taken at the 0,0 peaks of the absorption bands measured in chloroform.

configuration in which an electron is promoted from HOMO to LUMO. In addition, the orbital energy difference between HOMO and LUMO is still an approximate estimate to the transition energy since the transition energy also contains significant contributions from some two-electron integrals. However, because the HOMO−LUMO gap is easy to obtain, the approach can be used to estimate band gaps of large systems.

The theoretical parameter for direct comparison with experimental band gaps should be the transition (or excitation) energy from the ground state to the first excited state. The TDDFT method, which has been used to study systems of increasing complexity due to its relatively low computational cost and also to its inclusion, in its formalism, of the electron correlation effects, has been employed in this work. The excitation energy and the corresponding molecular orbitals involved for the $S_1 \leftarrow S_0$ and $S_2 \leftarrow S_0$ electronic transitions are compiled in Table 2. From these calculations, it is found that the first electronic transition ($S_1 \leftarrow S_0$) of each derivative is weakly allowed (small values of f), whereas the $S_2 \leftarrow S_0$ electronic transition possesses an oscillator strength 1 order of magnitude larger than the latter. Both transitions have $\pi \rightarrow \pi^*$ character, the first one having a dominant HOMO−LUMO excitation contribution, whereas the $S_2 \leftarrow S_0$ electronic transition is mainly described by the promotion of one electron from the HOMO−1 to the LUMO.

For **M1**, our theoretical calculations predict one weak electronic transition ($S_1 \leftarrow S_0$) at 26352 cm^{-1} ($f = 0.039$) and an intense electronic transition ($S_2 \leftarrow S_0$) at 31285 cm^{-1} ($f = 0.36$). The replacement of the primary alkyl chains by the secondary alkyl chains on the nitrogen atoms (**M1** vs **M2**) does not change the excitation energy of these derivatives much. Indeed, one can detect a very small decrease in the excitation energies of **M2** as compared to those of **M1**, with very small variations in the oscillator strenghts of both transitions (see Table 2). On the other hand, the incorporation of phenyl groups as side chains (**M3** and **M4**) or thiophene moieties (**M5**) induces increases in the excitation energies. Finally, one can see that the change of the substitution pattern on the phenyl rings (meta vs para) does not significantly affect the transition energies of these molecules. It is worth pointing out that the variations observed for the first electronic transition agree with the computed HOMO−LUMO energy gaps reported in Table 2.

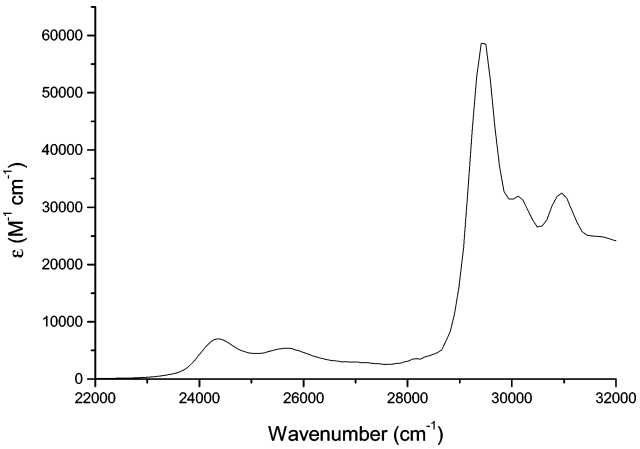

Figure 4. Absorption spectrum of M3 recorded in chloroform.

The absorption spectra of the compounds (the ethyl chains have been replaced by hexyl groups to achieve a better solubility) have been recorded in dilute chloroform solutions. As expected from theoretical calculations reported previously, the overall absorption profile of the derivatives are very similar. Figure 4 shows the absorption spectrum of **M3**, which is representative of all the spectra recorded. The 0,0 absorption peaks of the first and second electronic transitions of the five derivatives are reported in Table 2. It is worth pointing out that the length of the alkyl chains should not significantly affect the energies of the electronic transitions of these oligomers.[23]

One can see that the absorption spectrum profile of each derivative is well-described by these theoretical data. Indeed, each spectrum consists of one weak band in the long wavelength region followed by a more intense band in the UV region. The weak absorption band should correspond to the computed $S_1 \leftarrow S_0$ electronic transition, whereas the more intense band can be assigned to the second electronic excitation. It is worth pointing out that all absorption spectra exhibit several vibronic peaks, where the 0−,0 vibronic band of each electronic transition is the most intense. These results are typical of planar conjugated systems, which is obviously the case for these bridged carbazole derivatives.

TABLE 3: Optimized Bond Lengths (in Angstroms) of M3 in S_0 and S_1 States Calculated by DFT/6-31G* and RCIS/6-31G* Theoretical Methods, Respectively

	M3	
bond length	S_0	S_1
N_7-C_6	1.398	1.380
N_7-C_8	1.404	1.392
C_1-C_2	1.394	1.395
C_1-C_6	1.398	1.377
C_2-C_3	1.406	1.403
C_3-C_4	1.392	1.374
C_4-C_5	1.399	1.415
C_5-C_6	1.419	1.432
C_5-C_9	1.448	1.397
C_8-C_9	1.426	1.446
C_9-C_{10}	1.398	1.437
$C_{10}-C_{11}$	1.392	1.360
$C_{11}-C_{12}$	1.426	1.446
$C_{12}-C_{13}$	1.398	1.437
$C_{12}-C_{14}$	1.448	1.398
$C_{11}-N_{16}$	1.405	1.392
$C_{14}-C_{15}$	1.419	1.432
$C_{14}-C_{20}$	1.400	1.416
$C_{15}-N_{16}$	1.398	1.379
$C_{15}-C_{17}$	1.397	1.377
$C_{17}-C_{18}$	1.394	1.395
$C_{18}-C_{19}$	1.405	1.402
$C_{19}-C_{20}$	1.392	1.374

As can be seen in Table 2, the $S_1 \leftarrow S_0$ and $S_2 \leftarrow S_0$ excitation energies are computed at higher energies than those obtained from the 0,0 absorption peaks measured in chloroform. But, it is worth pointing out that our TDDFT calculations give the (0,0) transition energy equivalent to that in the gas phase. For this type of molecule, a bathochromic shift of at least 1000 cm^{-1} has to be assumed for the solvent shift, which should improve the agreement between experimental and computed excitation energies.[63] Moreover, it is observed that the computed differences in energy between the first and the second excitations are in excellent agreement with the experimental data reported in Table 2.

The optical absorption energies of **M1** and **M2** are found to be identical (see Table 2). From TDDFT calculations, a very small blue shift was predicted for the $S_1 \leftarrow S_0$ and $S_2 \leftarrow S_0$ electronic transitions of **M2** as compared to those of **M1**. These results clearly show that the substitutional pattern of the aliphatic chains (primary vs secondary) on the nitrogen atoms does not significantly change the transition energies of these chromophores. On the other hand, the replacement of primary alkyl chains by phenyl rings (**M3**) or thiophene groups (**M5**) on the nitrogen atoms induces hypsochromic shifts of the absorption bands, which are reproduced by TDDFT calculations (see Table 2). Finally, either TDDFT calculations or optical measurements show that the substitutional pattern of the phenyl rings (**M3** vs **M4**) does not significantly affect the excitation energies.

3.5. Excited-State (S_1) Geometry. Up to now, the standard for calculating excited-state equilibrium properties of large molecules is the configuration interaction singles (CIS) method. In this study, we have investigated the excited-state properties of the five indolocarbazoles by this method. In Table 3, we take **M3** as an example to compare the S_1 excited structure by CIS/6-31G* with its ground-state structure by DFT/B3LYP/6-31G*. It is apparent that the equilibrium geometries of the electronic ground state and of the S_1 state slightly differ. For instance, one can see in Table 3 that the C_1-C_6, C_3-C_4, C_5-C_9, $C_{10}-C_{11}$, $C_{12}-C_{14}$, $C_{15}-C_{17}$, and $C_{19}-C_{20}$ bond distances are shortened, whereas the C_4-C_5, C_5-C_6, C_8-C_9, C_9-C_{10}, $C_{11}-C_{12}$, $C_{12}-C_{13}$, $C_{14}-C_{15}$, and $C_{14}-C_{20}$ bond lengths are stretched. This suggests that, in the excited state, the molecules become more quinoid-like. A similar observation has been reported recently for oligofluorenes[26,64] and carbazole-based dyads.[27] It is also observed that, in the S_1 state, the 19−17−7−6 and 20−18−16−15 dihedral angles of **M2** are very similar to those found when the molecule is in the ground state. On the other hand, the phenyl rings in **M3** and **M4** become more twisted (19−17−7−6 and 20−18−16−15 = 72° as compared to 55° for the ground state) when the molecules are excited to the S_1 state.

TABLE 4: Emission Energies (E ($S_1 \rightarrow S_0$)) of Indolocarbazoles as Obtained by TDDFT Performed on RCIS/6-31G* Optimized Geometries of S_1 Excited States[a]

molecule	emission energy cm^{-1}	f[b]	Stokes shift[c] (cm^{-1})	E_f (cm^{-1})
M1	25 682	0.060	670	23 500
M2	25 525	0.077	633	23 600
M3	26 087	0.098	398	24 000
M4	26 247	0.097	256	24 100
M5	27 071	0.12	628	24 700

[a] Experimental emission energies (0,0 fluorescence peaks in chloroform) are given in the last column. [b] Oscillator strength of the $S_1 \rightarrow S_0$ electronic transition. [c] Energy difference between absorption (taken from Table 1) and emission energies.

3.6. Emission Transition Energies and Correlation with the Fluorescence Spectra. From the optimized (relaxed) S_1-state geometries, the $S_1 \rightarrow S_0$ transition energies were derived by means of the TDDFT approach (over the RCIS/6-31G* geometry), and the results are compiled in Table 4. For all the oligoindolocarbazoles, it is observed that, after relaxation (optimization) of the S_1 excited state, the energy of the first electronic transition decreases (see Tables 2 and 4). This transition should correspond to the emission energy of the derivatives. Indeed, the absorption of a photon excites the molecules to the S_1 Franck−Condon state, which should possess the ground-state (S_0) geometry. After the excitation, the molecules should relax to their most stable geometry before the emission process could occur to reach the S_0 Franck−Condon state, which possesses the S_1 relaxed geometry. As observed for excitation energies, the emission energy becomes slightly lower with the incorporation of secondary alkyl chains and becomes higher with the incorporation of phenyl and thiophene rings on the nitrogen atoms. Moreover, TDDFT calculations give a very small Stokes shift, as a consequence of the rigid planar geometries in the S_0 and S_1 states.

Figure 5 shows the fluorescence spectrum as well as the first absorption band of **M3**, which are representative of the spectra of the five compounds, in dilute chloroform solution. Their spectral characteristics are reported in Table 5. As expected for rigid planar systems, absorption and fluorescence spectra have nearly mirror-image profiles and exhibit several vibronic features; this indicates the same nature of the absorbing and emitting electronic state. Moreover, the vibronic features of the normalized emission spectra were found to be identical on exciting at different wavelength, indicating the presence of a single emitting species. Finally, as predicted from theoretical calculations, all compounds exhibit a small Stokes shift, which testifies the rigidity of these ladder compounds.

One can see in Table 4 that the fluorescence peaks of the carbazole derivatives are in relatively good agreement with the computed emission energies. In accordance with the absorption experiments, the fluorescence spectrum of **M2** appears at about the same energy (small blue shift of 100 cm^{-1}) as compared to that of **M1**. Moreover, as observed in absorption measurements,

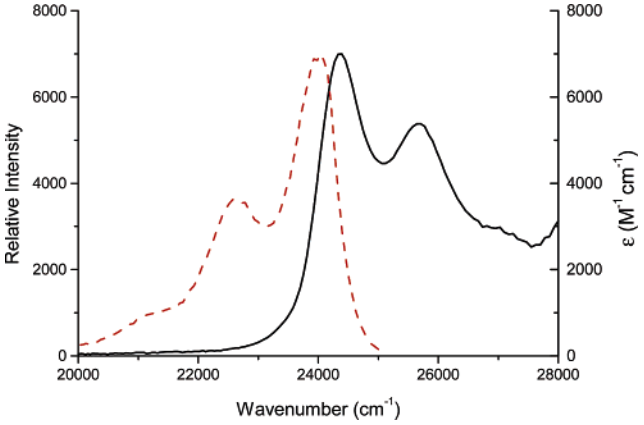

Figure 5. Absorption (—) and fluorescence (- - -) spectra of **M3** in chloroform. The fluorescence intensity has been normalized relative to the absorption band.

TABLE 5: Spectroscopic Parameters of Indolocarbazoles in Chloroform at Room Temperature (298 K)

molecule	λ_A[a] (nm)	ν_A[b] (cm^{-1})	ϵ[c] (M^{-1} cm^{-1})	λ_F[d] (nm)	ν_F[e] (cm^{-1})	Stokes shift[f] (cm^{-1})
M1	419	23 900	6500	425	23 500	400
M2	419	23 900	6600	423	23 600	300
M3	410	24 400	7000	416	24 000	400
M4	409	24 500	5600	415	24 100	400
M5	398	25 100	5700	405	24 700	400

[a] Absorption wavelengths taken at the maximum of the 0,0 vibronic peak. [b] Absorption wavenumbers taken at the maximum of the 0,0 vibronic peak. [c] Absorption coefficient at the maximum of the of the 0,0 vibronic peak. [d] Fluorescence wavelengths at the maximum of the 0,0 vibronic peak. [e] Fluorescence wavenumbers at the maximum of the 0,0 vibronic peak. [f] Energy difference between absorption and fluorescence 0,0 vibronic peaks.

TABLE 6: Photophysical Properties of Indolocarbazoles in Chloroform at Room Temperature (298 K)

molecule	ϕ_F	τ_F (ns)	10^{-8} k_F[a] (s^{-1})	10^{-8} k_{nr}[b] (s^{-1})
M1	0.13	2.90	0.45	3.0
M2	0.16	3.05	0.53	2.8
M3	0.14	3.69	0.38	2.3
M4	0.14	3.62	0.39	2.4
M5	0.023	0.63	0.37	16

[a] $k_F = \phi_F/\tau_F$. [b] $k_{nr} = k_F(1 - \phi_F)/\phi_F$.

the incorporation of phenyl rings (**M3** and **M4**) or thiophene moieties (**M5**) on the nitrogen atoms induces blue shifts in the fluorescence spectra.

3.7. Molecular Photophysics. The relevant results characterizing the photophysical properties presently studied are collected in Table 6. The values of the rate constants for radiative (k_F) and nonradiative (k_{nr}) decay were calculated according to the following expressions: $k_F = \phi_F/\tau_F$ and $k_{nr} = (1 - \phi_F)/\tau_F$, where ϕ_F and τ_F are the fluorescence quantum yield and lifetime, respectively. In all cases, τ_F was found to be independent of the excitation wavelength and the wavelength at which the emission is collected. Moreover, all fluorescence decays have been described as monoexponential with good statistical goodness-of-fit criteria ($\chi^2 < 1.3$ and DW ≈ 1.7), further confirming the presence of a single emitting species for each derivative.

For all the derivatives, it was found that the radiative decay rate constant was relatively weak, which goes along with the weak oscillator strengths (f) observed for the $S_1 \rightarrow S_0$ electronic transition (see Table 4). Consequently, all derivatives show relatively low fluorescence quantum yield (ϕ_F) values. Furthermore, one can see that the ϕ_F values of **M1** to **M4** are very similar. However, Table 6 shows that **M3** possesses a significantly longer τ_F value than **M1**, giving rise to a smaller k_{nr} value for **M3**. Moreover, it is found that the change of the substitutional pattern of the phenyl rings (**M3** vs **M4**) does not affect either radiative or nonradiative relaxations.

Finally, Table 6 shows that ϕ_F and τ_F of **M5** are much smaller than those of **M1** giving rise to a higher value of k_{nr} for **M5**. For thiophene derivatives, it is well-established that the main deactivation pathway of the S_1 state involves an intersystem crossing process (k_{isc}) due to the presence of the heavy sulfur atoms.[65,66] The same behavior is expected here for **M5** and might strongly contribute to the deactivation of the fluorescence.

Conclusion

A combined theoretical and experimental study of five ladder oligoindolocarbazoles functionalized on the nitrogen atoms was carried out. It was found that the side chains were twisted in the equilibrium geometry of the molecules, with relatively high rotational energy barriers against planarity. This should prevent the planarization of the side chains at ambient temperature. In their lowest singlet excited states, the five compounds investigated become more quinoid-like (RCIS results).

For all five compounds, the first electronic transition was a weakly dipole allowed (small values of f) $\pi\pi^*$ transition, which is dominated by the HOMO−LUMO excitation. Accordingly, the energy of the $S_1 \leftarrow S_0$ electronic transition follows the HOMO−LUMO energy gap of each compound. On the other hand, the $S_2 \leftarrow S_0$ electronic transition of each derivative possesses a much larger oscillator strength and is mainly described by the promotion of one electron from the HOMO−1 to the LUMO. Reasonable agreement is obtained between TDDFT calculations and measured spectral features.

The relaxation (optimization) of the excited states induces a lowering of the first electronic transition of the derivatives. Emission transition energies are relatively well-reproduced by TDDFT vertical transition energies computed from the S_1 optimized geometries (RCIS/6-31G*). Moreover, TDDFT calculations give a small Stokes shift, as a consequence of the similar geometries in the S_0 and S_1 states. The nature of the alkyl chains (primary vs secondary) on the nitrogen atoms does not significantly affect the spectroscopic parameters of the compounds. The replacement of aliphatic chains by phenyl or thiophene rings, as side chains, induces blue shifts in the absorption and fluorescence spectra. These spectral shifts are reproduced by TDDFT calculations. Moreover, it is found that the change of the substitutional pattern of the phenyl rings on the nitrogen atoms does not influence the transition energies.

Finally, the fluorescence quantum yields of the compounds investigated were relatively low and similar to each other, showing that the nature of the side chains on the nitrogen atoms does not have a great impact on the photophysical properties of these compounds. The sole exception is **M5**, which shows a much smaller ϕ_F value. One explanation for this behavior might be an enhancement of the intersystem crossing process caused by the presence of heavy sulfur atoms.

Acknowledgment. This work was supported by strategic and research grants from NSERC.

References and Notes

(1) Brabec, C. J.; Sariciftci, N. S.; Hummelen, J. C. *Adv. Funct. Mater.* **2001**, *11*, 15.

(2) Wienk, M. M.; Kroon, J. M.; Verhees, W. J. H.; Knol, J.; Hummelen, J. C.; van Hal, P. A.; Janssen, R. A. J. *Angew. Chem., Int. Ed.* **2003**, *42*, 3371.

(3) Padinger, F.; Rittberger, R. S.; Sariciftci, N. S. *Adv. Funct. Mater.* **2003**, *13*, 85.
(4) Dimitrakopoulos, C. D.; Malenfant, P. R. L. *Adv. Mater.* **2002**, *14*, 99.
(5) Katz, H. E. *Chem. Mater.* **2004**, *16*, 4748.
(6) Muccini, M. *Nat. Mater.* **2006**, *5*, 605−613.
(7) Leclerc, M. *J. Polym. Sci., Part A: Polym. Chem.* **2001**, *39*, 2867.
(8) Morin, J. F.; Leclerc, M.; Adès, D.; Siove, A. *Macromol. Rapid Commun.* **2005**, *26*, 761.
(9) Witte, G.; Wöll, C. *J. Mater. Res.* **2004**, *19*, 1889.
(10) Wang, C. S. *Trends Polym. Sci.* **1993**, *1*, 199.
(11) Babel, A.; Jenekhe, S. A. *J. Am. Chem. Soc.* **2003**, *125*, 13656.
(12) Alam, M. M.; Jenekhe, S. A. *J. Phys. Chem. B* **2002**, *106*, 11172.
(13) Brédas, J. L.; Beljonne, D.; Coropceanu, V.; Cornil, J. *Chem. Rev.* **2004**, *104*, 4971.
(14) Winder, C.; Saridifti, N. S. *J. Mater. Chem.* **2004**, *14*, 1077.
(15) Coakley, K. M.; McGehee, M. D. *Chem. Mater.* **2004**, *16*, 4533.
(16) Hoppe, H.; Sariciftci, N. S. *J. Mater. Res.* **2004**, *19*, 1924.
(17) Bouchard, J.; Wakim, S.; Leclerc, M. *J. Org. Chem.* **2004**, *69*, 5705.
(18) Wakim, S.; Bouchard, J.; Simard, M.; Drolet, N.; Tao, Y.; Leclerc, M. *Chem. Mater.* **2004**, *16*, 4386.
(19) Blouin, N.; Michaud, A.; Wakim, S.; Boudreault, P.-L. T.; Leclerc, M.; Vercelli, B.; Zecchin, S.; Zotti, G. *Macromol. Chem. Phys.* **2006**, *207*, 166.
(20) Wu, Y.; Li, Y.; Gardner, S.; Ong, B. S. *J. Am. Chem. Soc.* **2005**, *127*, 614.
(21) Li, Y.; Wu, Y.; Gardner, S.; Ong, B. S. *Adv. Mater.* **2005**, *17*, 849.
(22) Li, Y.; Wu, Y.; Ong, B. S. *Macromolecules* **2006**, *39*, 6521.
(23) Belletête, M.; Beaupré, S.; Bouchard, J.; Blondin, P.; Leclerc, M.; Durocher, G. *J. Phys. Chem. B* **2000**, *104*, 9118.
(24) Belletête, M.; Morin, J.-F.; Beaupré, S.; Ranger, M.; Leclerc, M.; Durocher, G. *Macromolecules* **2001**, *34*, 2288.
(25) Belletête, M.; Morin, J.-F.; Beaupré, S.; Leclerc, M.; Durocher, G. *Synth. Met.* **2002**, *126*, 43.
(26) Tirapattur, S.; Belletête, M.; Leclerc, M.; Durocher, G. *J. Mol. Struct.* **2003**, *625*, 141.
(27) Belletête, M.; Bédard, M.; Leclerc, M.; Durocher, G. *J. Mol. Struct.* **2004**, *679*, 9.
(28) Belletête, M.; Morin, J. F.; Leclerc, M.; Durocher, G. *J. Phys. Chem. A* **2005**, *109*, 6953.
(29) Belletête, M.; Durocher, G.; Hamel, S.; Côté, M.; Wakim, S.; Leclerc, M. *J. Chem. Phys.* **2005**, *122*, 104303.
(30) Belletête, M.; Wakim, S.; Leclerc, M.; Durocher, G. *J. Mol. Struct.* **2006**, *760*, 147.
(31) Frisch, M. J.; Trucks, G. W.; Schlegel, H. B.; Scuseria, G. E.; Robb, M. A.; Cheeseman, J. R.; Montgomery, J. A.; Vreven, T., Jr.; Kudin, K. N.; Burant, J. C.; Millam, J. M.; Iyengar, S. S.; Tomasi, J.; Barone, V.; Mennucci, B.; Cossi, M.; Scalmani, B.; Rega, G. N.; Petersson, G. A.; Nakatsuji, H.; Hada, M.; Ehara, M.; Toyota, K.; Fukuda, R.; Hasegawa, J.; Ishida, M.; Nakajima, T.; Honda, Y.; Kitao, O.; Nakai, H.; Klene, M.; Li, X.; Knox, J. E.; Hratchian, H. P.; Cross, J. B.; Adamo, C.; Jaramillo, J.; Gomperts, R.; Stratmann, R. E.; Yazyev, O.; Austin, A. J.; Cammi, R.; Pomelli, C.; Ochterski, J. W.; Ayala, P. Y.; Morokuma, K.; Voth, G. A.; Salvador, P.; Dannenberg, J. J.; Zakrzewski, V. G.; Dapprich, S.; Daniels, A. D.; Strain, M. C.; Farkas, O.; Malick, D. K.; Rabuck, A. D.; Raghavachari, K.; Foresman, J. B.; Ortiz, J. V.; Cui, Q.; Baboul, A. G.; Clifford, S.; Cioslowski, J.; Stefanov, B. B.; Liu, G.; Liashenko, A.; Piskorz, P.; Komaromi, I.; Martin, R. L.; Fox, D. J.; Keith, T.; Al-Laham, M. A.; Peng, C. Y.; Nanayakkara, A.; Challacombe, M.; Gill, P. M. W.; Johnson, B.; Chen, W.; Wong, M. W.; Gonzalez, C.; Pople, J. A. *Gaussian 03*; Gaussian, Inc.: Pittsburgh PA, 2003.
(32) Hohenberg, P.; Kohn, W. *Phys. Rev. B* **1964**, *136*, 864.
(33) Kohn, W.; Sham, L. J. *Phys. Rev. A* **1965**, *140*, 1133.
(34) Becke, A. D. *J. Chem. Phys.* **1993**, *98*, 5648.
(35) Lee, C.; Yang, W.; Parr, R. G. *Phys. Rev. B* **1988**, *37*, 785.
(36) Ditchfield, R.; Hehre, W. J.; Pople, J. A. *J. Chem. Phys.* **1971**, *54*, 724.
(37) Tretiak, S.; Mukamel, S. *Chem. Rev.* **2002**, *102*, 3171.
(38) Casida, M. E. In *Recent Advances in Density Functional Methods, Part I*; Chong, D. P., Ed.; World Scientific: Singapore, 1995; p 155.
(39) Gross, E.; Dobson, J.; Petersilka, M. *Top. Curr. Chem.* **1996**, *181*, 81.
(40) Wilberg, K. B.; Stratmann, R. E.; Frisch, M. J. *Chem. Phys. Lett.* **1998,** *297*, 60.
(41) Adamo, C.; Barone, V. *Chem. Phys. Lett.* **2000,** *330*, 152.
(42) Bruel, R.; Amos, R. D.; Handy, N. C. *Chem. Phys. Lett.* **2002**, *355*, 8.
(43) Yu, J. S. K.; Chen, W. C.; Yu, C. H. *J. Phys. Chem. A* **2003**, *107*, 4268.
(44) Foresman, J. B.; Head-Gordon, M.; Pople, J. A.; Frisch, M. J. *J. Phys. Chem.* **1992**, *96*, 135.
(45) Yudina, L. N.; Bergman, J. *Tetrahedron* **2003**, *59*, 1265−1275.
(46) Lin, C. H.; Tour, J. *J. Org. Chem.* **2002**, *67*, 7761−7768.
(47) Gong, L. Z.; Hu, Q. S.; Pu, L. *J. Org. Chem.* **2001**, *66*, 2358−2367.
(48) Abe, T.; Yamaji, T.; Kitamura, T. *Bull. Chem. Soc. Jpn.* **2003**, *76*, 2175−2178.
(49) Marzoni, G.; Garbrecht, W. L. *Synthesis* **1987**, 651−653.
(50) Grosu, I.; Ple, G.; Mager, S.; Mesaros, E.; Dulau, A.; Gego, C. *Tetrahedron* **1998**, *54*, 2905−2916.
(51) Cammidge, A. N.; Crepy, K. V. L. *J. Org. Chem.* **2003**, *68*, 6832−6835.
(52) Clayden, J. *Tetrahedron* **2004**, *60*, 4335−4335.
(53) Zhang, H.; Cai, Q.; Ma, D. *J. Org. Chem.* **2005**, *70*, 5164−5173.
(54) Ma, D.; Cai, Q. *Synlett* **2004**, 128−130.
(55) Eaton, D. F. *Pure Appl. Chem.* **1988**, *60*, 1107.
(56) Zelent, B.; Ganguly, T.; Farmer, L.; Gravel, D.; Durocher, G. *J. Photochem. Photobiol., A* **1991**, *56*, 165.
(57) Walker, S. D.; Barder, T. E.; Martinelli, J. R.; Buchwald, S. L. *Angew. Chem., Int. Ed.* **2004**, *43*, 1871−1876.
(58) Wilson, S. R.; Jacob, L. A. *J. Org. Chem.* **1986**, *51*, 4833−4836.
(59) Reich, H. J.; Whipple, W. L. *Can. J. Chem.* **2005**, *83*, 1577−1587.
(60) Boudreault, P.-L. T.; Wakim, S.; Blouin, N.; Simard, M.; Belletête, M.; Durocher, G.; Tao, Y.; Leclerc, M., manuscript submitted.
(61) De Oliveira, M. A.; Duarte, H. A.; Pernaut, J.-M.; De Almeida, W. B. *J. Phys. Chem. A* **2000**, *104*, 8256.
(62) Brière, J. F.; Côté, M. *J. Phys. Chem. B* **2004**, *108*, 3123.
(63) Belletête, M.; Leclerc, M.; Durocher, G. *J. Phys. Chem* **1994**, *98*, 9450.
(64) Gong, Z.; Lagowski, J. B. *J. Mol. Struct.* **2005**, *729*, 211.
(65) Becker, R. S.; Seixas De Malo, J.; Maçanita, A. L.; Elisei, F. *Pure Appl. Chem.* **1995**, *87*, 9.
(66) Rossi, R.; Ciofalo, M.; Carrita, A.; Ponterini, G. *J. Photochem. Photobiol., A* **1993**, *70*, 59.